Does grain size have an influence on intrinsic mechanical properties and conduction mechanism of near fully-dense boron carbide ceramics?

Bibi Malmal Moshtaghioun [a*], Miguel Angel Laguna-Bercero[a], Diego Gómez-García [b] and Jose I. Peña [a]

[a] Instituto de Ciencia de Materiales de Aragón, CSIC-Universidad de Zaragoza, campus Río Ebro, 50018 Zaragoza, Spain

[b] Instituto de Ciencia de Materiales de Sevilla, CSIC-Departamento de Física de la Materia Condensada, Universidad de Sevilla, 41092 Sevilla, Spain.

* Corresponding author:

Bibi Malmal Moshtaghioun
Instituto de Ciencia de Materiales de Aragón, Universidad de Zaragoza, campus Río Ebro, Zaragoza, Spain.
Phone: +34-876555601 (845601)
E-mail: mali@unizar.es, mali_moshtagh@us.es

Abstract

This work is concentrated on getting a reply to the following question: how does the grain size of boron carbide specimens influence on their mechanical and electrical response? It is a common issue that both essential properties are usually affected by the grain boundaries. To this purpose, a set of near fully-dense boron carbide specimens were prepared by spark plasma sintering. In order to reduce residual porosity and grain-size effects, nanoindentation tests at room temperature were conducted. DC conductivity was measured through four-point test technique from room temperature up to 800ºC. The results show that hardness can reach values as high as ~60 GPa and plasticity onset takes place at around 23 GPa by dislocation nucleation. Regarding the conductivity, it is found that grain boundaries can block the mobility of bipolarons in an effective way. A simple additive law is provided to account for the resistivity of boron

carbide polycrystals.

Keywords: boron carbide; grain size dependence; nanoindentation; electrical conductivity

1. Introduction

Boron carbide (B_4C) ceramic is the third hardest material after diamond and cubic boron nitride. It exhibits many attractive properties, such as a high elastic modulus and wear resistance combined with a low density. Regarding their electrical properties, it is well-known as a reasonably good semiconductor at high temperatures [1-12].

Because of the high potential applications, investigation of both mechanical and electrical properties at conditions which are close to those experienced in service are of special interest. To this end, an accurate analysis of hardness and elastic modulus as well as conductivity and their grain size dependence is essential for advanced applications. In this sense, previous studies have shown a relatively wide range of hardness values by Vickers indentation ~20-35 GPa [3-13] and nano-indentation ≥ 40GPa as well as elastic modulus ≥500GPa [14-19]. This large variation is mainly related to the presence of porosity in boron carbide ceramics, their grain-size effects, the composition and the indentation load. Consequently, it is difficult to give a clear response to the grain size dependence of hardness and elastic modulus without the influence of other parameters. Regarding conductivity, this material is the paradigm of a semi-conductor with hopping conduction mechanism by small bipolarons hopping [20-23]. However, the grain size dependence on the conductivity in boron carbide has not been previously reported.

In this study, grain size dependence of hardness and elastic modulus were investigated by the nano-indentation method to minimize the drawback of residual porosity and grain-size effects on these properties. In consequence, intrinsic mechanical properties can be measured and these ones can be compared with those already reported to evaluate the grain-size effects. Furthermore, the effect of grain size on the electrical properties of B_4C from room-temperature up to 800ºC was also assessed.

2. Experimental procedure

Three available boron carbide powders with average particle size around 500 nm, 220 nm and 40 nm (Grade HD20, High-energy ball milled of Grade HD20, H. C. Starck, Germany and Tekna Plasma System Inc., Canada, respectively) were used as the starting materials. The characterization of impurity content and the powder preparation is reported elsewhere [10-12]. Regarding the possible role of minority impurities, particularly iron, previous works in literature [24, 25] discarded any influence on densification and physical properties, particularly electrical or mechanical ones. Recent achievements by Hu et al. [26] have showed that ion milling can introduce some impurities that could degrade the mechanical properties of hot-pressed specimens at temperatures as high as 2050ºC. This is not our case, since our sintering temperatures are much lower, as reported in Table 1. The powder was consolidated under vacuum in a SPS device (Dr. Sinter 515S, Kanagawa, Japan), using a cylindrical graphite die with an inner diameter equal to 15 mm. A pressure of 75 MPa was applied upon heating and cooling and released at the end of process. In all cases the heating rate was 100 ºC/min. During the sintering process, the temperature was measured by an optical pyrometer, which was focused on a bare hole in the middle part of the graphite die. Table 1 lists the specific SPS variables used and more details on processing and sample preparation are reported elsewhere [10-12].

The relative density of the sintered samples was measured by the Archimedes method, using distilled water as the immersion liquid. It was also measured from the weight and dimensions of parallelepipeds cut from the sintered specimens to assess the values provided by the Archimedes method, with a good agreement between them. Microstructural analysis was performed on both fractured and polished surfaces by scanning electron microscopy (HITACHI

S5200, Japan). The grain size was determined from the SEM pictures. The polished surfaces were electro-chemically etched with a solution of 1% KOH.

Hardness (H) and elastic modulus were measured by Nanoindentation tests (Agilent Technologies G200, U.S.A. equipped with a Berkovich indentor) on polished surfaces with constant loading rate of 0.5 mN/s. The values of hardness and elastic modulus were obtained by averaging 40 indentation tests at different positions to minimize the effects of sample surface roughness and grain orientations. Two different approaches were considered: first, maximum indentation load of 250 mN and second maximum penetration depth of 50nm and 100 nm were done as well, to measure hardness and elastic modulus from loading-unloading curves. Later ones were chosen to restrict the penetration depth to one grain even for the finest microstructure studied here.

The electrical conductivity was determined by the four-point probes method in a tubular furnace under Ar atmosphere from room temperature up to 800ºC using a heating/cooling rate of 2 ºC/min. Specimens with a size of 2.5 mm×2.5 mm×7mm were placed into a ProboStat^{TM} cell in order to perform the electrical measurements. A current of 500 mA was applied and the voltage was measured.

3. Results and discussion

3.1. SEM characterization

Figure 1 compares representative FE-SEM images of the B_4C ceramics considered in this study. Initial B_4C powder with 500 nm resulted in fully-dense boron carbide specimens at both SPS temperature of 1700 and 1800 ºC (Table. 1) while a coarse microstructure with average grain size of 25 μm was found at 1800 ºC (Fig. 1A). In contrast, lower SPS temperature of 1700 ºC is effective in retaining fine-grained microstructures and sub-micrometric boron carbide

specimens with average grain size of 700 nm were obtained (Fig. 1B). In the case of B_4C powder with 220 nm particle size, the relative densities were >98% and the microstructure had similar dependence with temperature (coarse microstructure with average grain size of 17 μm at 1800 ºC and sub-micrometric microstructure with average grain size of 370 nm at 1700 ºC) and there were only a few isolated pores in the microstructures (Fig. 1C-D). In the case of nano-B_4C powder, a lower sintering temperature of 1600 ºC and two-step SPS [12] was required to retain the nanostructured character and nano-grained B_4C ceramics with an average grain size of ~100 nm were obtained. Locally interconnected pores were present in the microstructure with no evidence of extended pore network (Fig. 1E) and the relative density was only 95%. The main important feature in all SEM images is the omnipresence of twins that is previously reported in boron carbide ceramics [13,27,28].

3.2. Mechanical properties

The experimental results of hardness and elastic modulus of all samples for 250 mN indentation load are listed in Table. 1. The hardness values were found between 33 to 49 GPa without any clear dependence on the grain size. A similar scatter of micro-hardness values was observed previously in Vickers indentations, which are shown in Table. 1 for comparison. In Vickers indentation, the indentation depth is more than 30 μm for HV2 (Load 20N) while in the case of nano-indentation, the displacement into the surface is around 650 nm in harder samples and 800 nm in less hard ones (Fig.2). This means that only for sub-micrometric and nano-grained samples, more than one grain is subjected to nano-indentation loads. Similar feature was observed regarding elastic modulus, i.e. they were ~400-550 GPa (Table. 1). Xie et. al. [16] reported large scatter of hardness (20-50 GPa in the case of 125 mN load and 25-54GPa for a 30

mN load) in stoichiometric boron carbide ceramics with 5-10 μm grain size due to the higher porosity of the sample (~18%) which is more prominent for larger indent and limited the highest hardness value. However, the porosity influence cannot be avoided even in very low nano-indentation loads [16]. This fact was observed in hardness values from Vickers [13] which is usually lower than the hardness measured by nanoindentation from the same samples. It is well-known that micro-cracks induced by Vickers hardness can be responsible for lower hardness and other microstructural defects like pores and intrinsic cracks also affect more because of larger loads and indentation imprint.

In order to eliminate the porosity influence on hardness and elastic modulus, porosity correction was carried out. For this purpose, models based on minimum solid area ($M_{true}=M_{exp}.Exp(bP)$: M is hardness or elastic modulus, b is a constant and P is porosity) [13,26] were used. For carbides, values for b of ~5-8 are common [29] and these correspond to various packing geometries of solid spheres in minimum solid area models (Fig. 5). Here, b=6 gives the most reasonable data. True data obtained after correction by nano indentor with 250mN load are listed in Table 1 and showed in Fig. 3. Assuming the validity of this correction, true data have similar values of hardness (46-49 GPa) and elastic modulus (525-565 GPa) independent on the grain size.

In order to minimize the porosity influence on hardness and elastic modulus data, nano-indentation tests were performed at a maximum penetration depth of 100 nm, which are displayed in Fig. 4. With lower displacement into the surface, hardness (57-64 GPa) and elastic modulus (624-684 GPa) were found to be practically grain size independent even without porosity correction. An example of a load-displacement curve at a maximum penetration depth of 100 nm for boron carbide sample with 700 nm grain size is shown in Fig. 5. Some important

features can be observed from the plot. First of all, the displacement was not smooth and several discontinuities and shape changes were found (Fig. 5) in comparison with smoother load-displacement curves performed using higher loads (Fig. 2). An abrupt increase of the imprint depth during loading (pop-in) was detected, as shown by arrows in Fig. 5. The presence of such steps (pop-in) under low loads (5mN) indicates the onset of plastic deformation and therefore the measured hardness is determined by nucleation of dislocations with/without twin interaction. These steps (pop-in) were observed in load-displacement curves at a maximum penetration depth of 100 nm for all boron carbide samples with different grain size. Furthermore, the presence of multiple pop-in events is characterized as a plastic deformation and also was previously observed in other semi-conductor materials [30, 31]. This statement is also consistent with quantative analysis. Following the procedure reported in [19], which is based upon the Oliver and Pharr analysis, the shear stress associated to these pop-in events for all boron carbide samples is approximately 23±5 GPa, and it does not depend on the grain size of the specimen. (In essence, the shear stress $\tau \cong 0.47P/A$, where P is the load recorded when pop-in takes place and A the effective area under the nanoindentor, which is calculated through the Oliver and Pharr technique procedure [32]). Since the theoretical shear strength in boron carbide is approximately $G/2\pi$ (being G the shear modulus) i.e. 32 GPa [19] the closeness of the value of the shear stress to the theoretical shear strength seems to indicate that nucleation of Frank-Read loops due to loss of stability of the lattice takes place. Multiple pop-ins confirm that dislocations with/without twin interactions can impede dislocation motion without recovery and resulted in work hardening effect in boron carbide. This is found to be the main mechanism of deformation in boron carbide, as previously reported [27,28]. Consequently, hardness reached higher values of ~57-64 GPa under low indentation loads. The evidence of tiny discontinuities on unloading curves (elbows)

indicates dislocation recovery after load release and support the deformation scenario proposed above. On the other side, disorder or amorphization of boron carbide during nano-indentation at high loads (250mN) can be responsible of the lower hardness values and smooth load-displacement curves in the same samples. This idea has been reported by other authors as well [14].

In the case of lower penetration depths up to 50 nm maximum, another feature arises and curves of loading and un-loading of the indenter are superimposed on one another, as shown in Fig. 6 for samples of 700 nm grain size. Here the indentation load is ~ 1mN. In this case, residual plastic imprint is reduced and they exhibited mostly an elastic behavior. However, the presence of pop-in and tiny deformation was also found (Arrow in Fig. 6).

3.3. Electrical conductivity

Regarding the electrical conductivity, the grain size dependence for the set of B_4C samples is displayed in Fig. 7. Comparable electrical conductivities of single crystals of boron carbide with the stoichiometric composition B_4C were reported before [20,23]. In the case of the polycrystalline materials studied in this work, conductivity decreases with decreasing grain-size. This is consistent with grain boundaries acting as barriers limiting the mobility of electrical carriers. Furthermore, the temperature dependence of the conductivities has a striking feature: the conductivities reach a maximum at a given temperature. However, the temperature at which this maximum value is obtained depends on the grain size. When grain size decreases, the temperature of maximum conductivity increases (Arrow in Fig. 7).

The temperature dependence of the electrical conductivity in boron carbide was modeled by Aselage et al. [22]. In the light of that model, conductivity is controlled by bipolaron hopping

[20, 23]. The conductivity depends on the fraction of occupied sites by bipolarons in boron-carbide icosahedrals (*f*). Such quantity exhibits a "non-Arrhenius" temperature dependence as shown:

$$\sigma T = A\frac{f(1-f)}{kT}\exp\left(\frac{-E}{kT}\right) \quad (1)$$

Where A is a constant, k the Boltzmann constant and E is an energy barrier for bipolaron hopping which depends on the difference of electronic energies of initial and final states in a hop [22]. Figure 8 displays the agreement with an Arrhenius dependence of σT versus the inverse of the temperature. The energy barrier is equal to 0.10±0.05 eV. This is in good agreement with the reported values in [22] (0.16 eV).

According to the model cited above, the bipolaron hopping is progressively suppressed when temperature (or polaron density) increases. At a given temperature, the fraction of mobile bipolarons reaches a maximum value. The theoretical law correlating the temperature and the maximum value of *f* was proposed in [22] from quantum mechanical analysis of the hopping process and the availability of permitted final states for the hopping bipolaron.

Such law adopts the following form:

$$\ln\frac{f}{f_0} = \frac{5}{8}\ln\left(\frac{T}{T_0}\right) + \frac{\varepsilon_B}{2kT_0}\left(\frac{T_0}{T} - 1\right) \quad (2)$$

Where T_0 is the temperature at which conductivity reaches its maximum value in single crystals or polycrystals with very large grain sizes and $\varepsilon_B \cong 0.3$ eV is the binding energy of bipolarons in boron carbide. The value of f_0 is the fraction of occupied sites by bipolarons in single crystals or polycrystals with very large grain sizes consequently.

In the frame of this model, a picture arises to give sense to our results: a significant ratio of bipolarons is blocked at the grain boundaries when the grain size decreases. At a given temperature, the conductivity decreases for smaller grain sizes because the contribution of grain boundaries to the ratio of available sites is higher in fine-grained specimens.

The undesired presence of grain boundaries provokes that the fraction of occupied sites decreases. Therefore, higher temperatures are required to increase their concentration up to the level in which hopping suppresses. Thus, the maximum of conductivity must be reached at much higher temperatures, when the density of these carriers increases.

A quantitative assessment of this interpretation is provided in Table 3. Making use of data displayed in Fig.7, the maximum values of the conductivities and the temperatures at which these maxima are found have been recorded. Equation (1) can be used to determine the experimental value of the quantity *f*. It was observed that the sample with the largest grain size (25 μm) shows results similar to those found in crystalline specimens. The temperature of its highest conductivity was T_0=634 K. On the other hand, equation (2) can provide the theoretical value of *f* once known it is the temperature at which the conductivity reaches the maximum value. This calculation can be carried out straightforwardly and the results are also provided in Table 3 for the sake of comparison. The agreement with our experimental data is fairly good support for this hypothesis.

Another aspect which deserves attention is the grain size (*d*) dependence of the electrical conductivity. Mayadas and Shatzkes [33] proposed an analytical model for the resultant resistivity (ρ) of one grain of columnar shape and length d and conclude that it can be expressed as:

$$\rho = \rho_0 + \frac{3}{2}\rho_0 \frac{\lambda}{d}\frac{R}{1-R} \tag{3}$$

Where ρ_0 is the resistivity of the bulk. Therefore, the second term after ρ_0 in equation (3) is the grain-boundary resistivity contribution. The symbol λ stands for the mean free path of the charge carriers and *R* is a reflection coefficient accounting for the scattering of holes at the grain boundaries. It is admitted that λ<<d (see equation (11) in reference [33]). Assuming this law, which validates the Mathiessen's rule, the resultant conductivity ($1/\sigma = 1/\sigma_0 + 1/\sigma_{gb}$), the sum of the bulk conductivity (σ_0) and the grain-boundary one (σ_{gb}), should fit to a dependence as shown here:

$$\frac{\sigma}{\sigma_0} = \frac{\alpha d}{1+\alpha d} \tag{4}$$

A simple comparison between Equations (3) and (4) allows concluding that the constant α in equation (4) is derived from λ and R as:

$$\alpha \cong \frac{2}{3}\frac{(1-R)}{R\lambda} \tag{5}$$

A plot of the electrical conductivity versus the grain size at a constant value of the temperature is provided in Fig. 9. The fitting to the law displayed in equation (4) is acceptable (r=0.97) and it provides a value for α which is given by α≅0.0029 nm^{-1}. The agreement with this law is a remarkable fact and it deserves a more theoretical insight into the mechanisms for conductivity. As commented previously, λ is the mean free path of the carriers and R a reflection coefficient of holes at the grain boundaries or structural defects. The reflexion coefficient is expected to reach values as high as *R*~0.95-0.99 in ceramics in which grain boundaries reduces notably the resultant conductivity [33]. Making use of equation (5), the mean free path is in-between 1-10 nm. Werheit and Gerlach [34] measured the infrared reflectivity of boron carbide and determined the hole mean free path, which is of the order of ~ 1-5-nm. This result is not a proof of validity

of the model but at least it shows a reasonable consistency. A more thorough theoretical analysis is required to go insight into the mechanisms of bipolaron conductivity in boron carbide, especially when intense twinning takes place. This task is exciting but a priori it seems to be very challenging.

4. Conclusions

Nanoindentation tests under controlled displacement have been carried out in near fully-dense boron carbide specimens prepared by spark plasma sintering. The tests show that hardness can reach values as high as 64 GPa. Nucleation of dislocations occurs when the local shear stresses are around 23 GPa, which is very close to the theoretical shear strength. Regarding electrical conductivity tests, grain boundaries are structural defects reducing the conductivity controlled by bipolaron motion. The temperature dependence of the conductivity is controlled by the density of unblocked bipolarons. The temperature at which conductivity reaches the maximum value increases when the grain size decreases, which is consistent with theoretical predictions previously reported.

Acknowledgements. This work was supported by the Ministerio de Economía y Competitividad (Government of Spain) and FEDER Funds under Grants No. MAT2015- 71411-R. and MAT77769-R. BMM wants to acknowledge the support of the Spanish MINECO by means of a "Juan de la Cierva-Incorporación" fellowship during her sabbatical stay in Zaragoza.

References

1. V. Domnich, S. Reynaud, R.A. Haber, M. Chhowalla, Boron carbide: structure, properties, and stability under stress, *J. Am.Ceram. Soc.* **94** (2011)3605–3628.
2. M. Chen, J.W. McCauley, K.J. Hemker, Shock-induced localized amorphization in boron carbide, *Science*. **299** (2003) 1563–1566.
3. R.F. Speyer, N. Cho, Z. Bao, Density- and hardness-optimized pressureless sintered and post-HIPed B_4C, *J. Mat. Res.***20**(8) (2005) 2110–2116.
4. D. Ghosh, G. Subhash, T.S. Sudarshan, R. Radhakrishnan, X.L. Gao, Dynamic indentation response of fine-grained boron carbide, *J. Am. Ceram. Soc.***90**(6) (2007) 1850–1857.
5. S. Hayun, V. Paris, M.P. Dariel, N. Frage, E. Zaretzky, Static and dynamic mechanical properties of boron carbide processed by spark plasma sintering, *J. Eur. Ceram. Soc.***29**(16) (2009) 3395–3400.
6. K.H. Kim, J.H. Chae, J.S. Park, J.P. Ahn, K.B. Shim, Sintering behavior and mechanical properties of B_4C ceramics fabricated by spark plasma sintering, *J. Ceram. Proc. Res*.**10**(6) (2009) 716–720.
7. A.K. Suri, C. Subramanian, J.K. Sonber, T.S.R-Ch Murthy, Synthesis and consolidation of boron carbide: a review, *Int. Mater. Rev.***55**(1) (2010) 4–40.
8. S. Hayun, S. Kalabukhov, V. Ezersky, M.P. Dariel, N. Frage, Microstructural characterization of spark plasma sintered boron carbide ceramics, *Ceram. Inter.* **36**(2) (2010) 451–457.
9. K. Madhav Reddy, J.J. Guo, Y. Shinoda, T. Fujita, A. Hirata, J.P. Singh, J.W. McCauley, M.W. Chen, Enhanced mechanical properties of nanocrystalline boron carbide by nanoporosiy and interface phases. *Nat .Commun.* **3** (2012) 1052.

10. B.M. Moshtaghioun, F.L. Cumbrera-Hernández, D. Gómez-García, S. de Bernardi-Martín, A. Domínguez-Rodríguez, A. Monshi, M.H. Abbasi, Effect of spark plasma sintering parameters on microstructure and room-temperature hardness and toughness of fine-grained boron carbide (B_4C), *J. Eur. Ceram. Soc.***33**(2) (2013) 361–369.
11. B.M. Moshtaghioun, F.L. Cumbrera-Hernández, A.L. Ortiz, M. Castillo-Rodríguez, D. Gómez-García, Additive-free superhard B_4C with ultrafine-grained dense microstructures. *J. Eur. Ceram. Soc*. **34**(3) (2014) 841–848.
12. B.M. Moshtaghioun, A.L. Ortiz, D. Gómez-García, A. Domínguez-Rodríguez, Densification of B_4C nanopowder with nanograin retention by spark-plasma sintering, *J. Eur. Ceram. Soc.***35**(6) (2015) 1991–1998.
13. B.M. Moshtaghioun, D. Gómez-García, A. Domínguez-Rodríguez, R.I. Todd, Grain size dependence of hardness and fracture toughness in pure near fully-dense boron carbide ceramics, *J. Eur. Ceram. Soc.* 36 (2016)1829–1834.
14. V. Domnich, Y. Gogotsi, M. Trenary, T. Tanaka, Nanoindentation and Raman spectroscopy studies of boron carbide single crystals, *Appl. Phys. Lett.* **81**(20) (2002) 3783–3785.
15. Ch. Cheng, K.M. Reddy, A. Hirata, T. Fujita, M. Chen, Structure and mechanical properties of boron-rich boron carbides, *J. Eur. Ceram. Soc.* 37 (2017) 4514–4523.
16. K.Y. Xie, V. Domnich, L. Farbaniec, B. Chen, K. Kuwelkar, L. Ma, J.W. McCauley, R.A. Haber, K.T. Ramesh, M. Chen, K.J. Hemker, Microstructural characterization of boron-rich boron carbide, Acta. Mat.136 (2017) 202-214.
17. L. Farbaniec, J. McCauley, J. Hogan, K. Ramesh, Anisotropy of mechanical properties in a hot-pressed boron carbide, Int. J. Appl. Ceram. Technol. 13 (2016) 1008-1016.
18. A. Richter, C.P. Daghlian, R. Ries, V.L. Solozhenko, Investigation of novel superhard

materials by multi-cycling nanoindentation, Diomond & Related. Mat. 15 (2006)2019-2023.

19. S.N. Dub, V.I. Kushch, O.N. Kaidash, V.P. Sereda, T.S. Panasyuk, Initiation of a plastic flow in boron carbide at nanoindentation, J. Superhard. Mat. 37 (2015) 8-13.
20. Ch. Wood, D. Emin, Conduction mechanism in boron carbide, Phys. Rev. B. 29 (1984) 4582-4587.
21. H. Werheit, Thermoelectric properties of boron-rich solids and their possibilities of technical application, 25th Int. Conf . Thermoelectr. (2006). P.159-163.
22. T.L. Aselage, D. Emin, S.S. McCready, Conductivities and Seebeck coefficients of boron carbides: softening bipolaron hopping, Phys. Rev. B. 64 (2001) 0543021-8.
23. S. Roszeitis, B. Feng, H.P. Martin, A. Michaelis; Reactice sintering process and thermoelectric properties of boron rich boron carbides, *J. Eur. Ceram. Soc.***34** (2014) 327-336.
24. H Werheit, S Shalamberidze, Advanced microstructure of boron carbide, 2012 J. Phys.: Condens. Matter 24 385406.
25. H Werheit, G Gerlach, Dynamical conductivity of boron carbide: heavily damped plasma vibrations, 2014 J. Phys.: Condens. Matter 26 425801.
26. J Hu, F Zhang, W Wang, Z Fu, J Zhang, Effect of impurities introduced by ball milling on hot pressed boron carbide, Journal of the European Ceramic Society 39 (2019) 2874–2881.
27. B.M. Moshtaghioun, D. Gómez-García, A. Domínguez-Rodríguez, N.P. Padture, High-temperature creep deformation of coarse-grained boron carbide ceramics, *J. Eur. Ceram. Soc.* **35**(5) (2015) 1423–1429.
28. B.M. Moshtaghioun, D. Gómez-Garcia, A. Domínguez-Rodríguez, High-temperature deformation of fully-dense fine-grained boron carbide ceramics: experimental facts and

modeling, *Mater. Des.* **88** (2015)287–93.

29. R.W. Rice, Evaluation and extension of physical property-porosity models based on minimum solid area. J. Mater. Sci. 31 (1996) 102-118.
30. J.E. Bradby, J.S. Williams, J. Wong-Leung, M.V. Swain, P. Munroe, Nanoindentation-induced deformation of Ge, App. Phys. Let. 80 (2002) 2651-2653.
31. J.E. Bradby, J.S. Williams, M.V. Swain, Pop-in events induced by spherical indentation in compound semiconductors, J. Mater. Res. 19 (2004) 380-386.
32. W.C. Oliver, G.M. Pharr, An improved technique for determining hardness and elastic modulus using load and displacement sensing indentation experiments, J. Mater. Res.7 (1992) 1564-1583.
33. A.F. Mayadas, M. Shatzkes, Electrical-resistivity model for polycrystalline films: the case of arbitrary reflection at external surfaces, Phys. Rev. B. 1 (1970) 1382-1389.
34. H. Werheit, G. Gerlach, Dynamical conductivity of boron carbide: heavily damped plasma vibrations, J. Phys. Conden. Matter. 26 (2014) 425801-8.

Figure Captions

Figure 1. Representative FE-SEM micrographs of B_4C ceramics (A) from powder with 500 nm particle size and SPS-ed at 1800 ºC, (B) from powder with 500 nm particle size and SPS-ed at 1700 ºC, (C) from powder with 220 nm particle size and SPS-ed at 1800 ºC, (D) from powder with 220 nm particle size and SPS-ed at 1700 ºC and (E) from powder with 40 nm particle size and SPS-ed at 1600 ºC .

Figure 2. Indenter load-displacement curves for boron carbides samples with different grain size at the maximum load of 250 mN.

Figure 3. Experimental and true (A) hardness and (B) elastic modulus at the maximum load of 250 mN as a function of inverse square root of grain size and grain size, respectively.

Figure 4. Experimental (A) hardness and (B) elastic modulus at maximum penetration depth of 100 nm as a function of inverse square root of grain size and grain size, respectively.

Figure 5. Load-displacement curve for boron carbide sample with 700 nm grain size at maximum penetration depth of 100 nm.

Figure 6. Load-displacement curve for boron carbide sample with 700 nm nm grain size at maximum penetration depth of 50 nm.

Figure 7. Plot of conductivity as a function of reciprocal temperature for boron carbides samples with different grain size.

Figure 8. Arrhenius dependence of σT versus the reciprocal temperature for the sets of boron carbide specimens under study.

Figure 9. Grain-size dependence of the electrical conductivity at a constant value of temperature equal to 634 K for the set of boron carbide specimens considered in this work. The fitting is based on the equation (3) proposed in the main text.

Table Captions

Table 1. Processing conditions, microstructural features and mechanical properties obtained by nanoindentation at the maximum load of 250 mN. The results from Vickers indentation are listed for comparison [13].

Table 2. Mechanical properties obtained by nanoindentation at a maximum penetration depth of 100 nm for the set of boron carbide samples studied here.

Table 3. Values of the conductivity at the temperatures in which maximum values are reached. The temperatures of these maxima are displayed as a function of the grain size. The experimental values of f obtained from equation (1) and the theoretical ones derived from equation (2) are also provided for the aim of a proper comparison. The values corresponding to the specimens with 100 μm grain size are not given because the temperature of the maximum is not within the temperature range of our experimental set-up

***Highlights (for review)**

- Nanoindentation and conductivity of B_4C ceramics from 25 μm to 100 nm grain size
- Hardness reaches values as high as 60 GPa which is practically grain size independent
- Plasticity onset is ~23 GPa by dislocation nucleation and close to shear strength
- Grain boundaries are structural defects reducing conductivity by bipolaron motion

Table

Table 1

Sample designation	Relative density	Ave. Grain size	Vickers hardness HV2 [13]		Nano-indentation with 250 mN load			
			Experimental Hardness (GPa)	True Hardness (GPa)	Experimental Hardness (GPa)	True Hardness (GPa)	Experimental Elastic modulus (GP)	True Elastic modulus (GPa)
500n[a]-SPS 1800 °C-3min	100	25 µm	29±2	29	48±2	48±2	526±16	526±16
220n[b]-SPS 1800 °C-3min	99.2	17 µm	29±2	31	44±4	47±4	509±46	534±46
500n[a]-SPS 1700 °C-3min	100	700 nm	34±2	34	49±3	49±3	552±24	552±24
220n[b]-SPS 1700 °C-3min	98.5	370 nm	33±1	36	42±2	46±2	507±13	555±13
40n[c]-SPS 1600 °C-1min	94.6	100 nm	27±1	40	33±4	46±4	404±34	565±34

[a] 500n denotes sub-micrometric B4C powders with average particle size of 500 nm.

[b]220n denotes sub-micrometric B4C powders with average particle size of 220 nm.

[c]40n denotes nano-B4C powders with average particle size of 40 nm.

Table 2

Sample designation	Relative density	Ave. Grain size	Nano-indentation with 100 nm displacement into surface	
			Experimental Hardness (GPa)	Experimental Elastic modulus (GP)
500n-SPS 1800 °C-3min	100	25 μm	59±4	635±26
220n-SPS 1800 °C-3min	99.2	17.2 μm	58±4	641±32
500n-SPS 1700 °C-3min	100	700 nm	64±5	684±43
220n-SPS 1700 °C-3min	98.5	370 nm	62±7	667±50
40n-SPS 1600 °C-1min	94.6	100 nm	57±7	624±55

Table 3

Grain size (μm)	Maximum value of conductivity (S/cm)	Experimental values of f/f_0	Theoretical values of f/f_0	T (K)	T/T_0
25	14.35	1	1	634	1
17	13.26	0.78	0.8	711	1.12
0.7	10.65	0.64	0.68	800	1.26
0.37	9.35	0.58	0.55	915	1.44

Figure

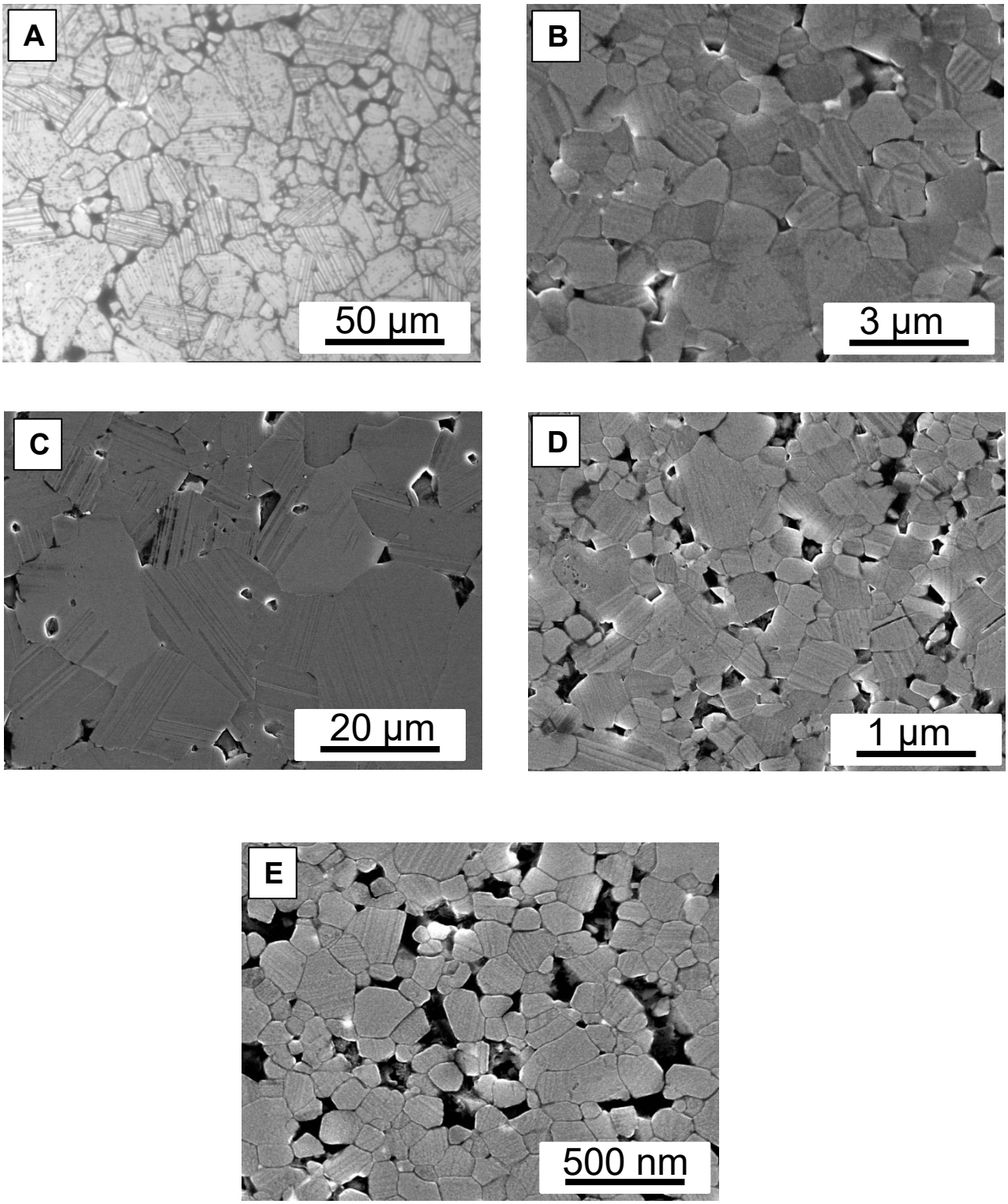

Fig. 1

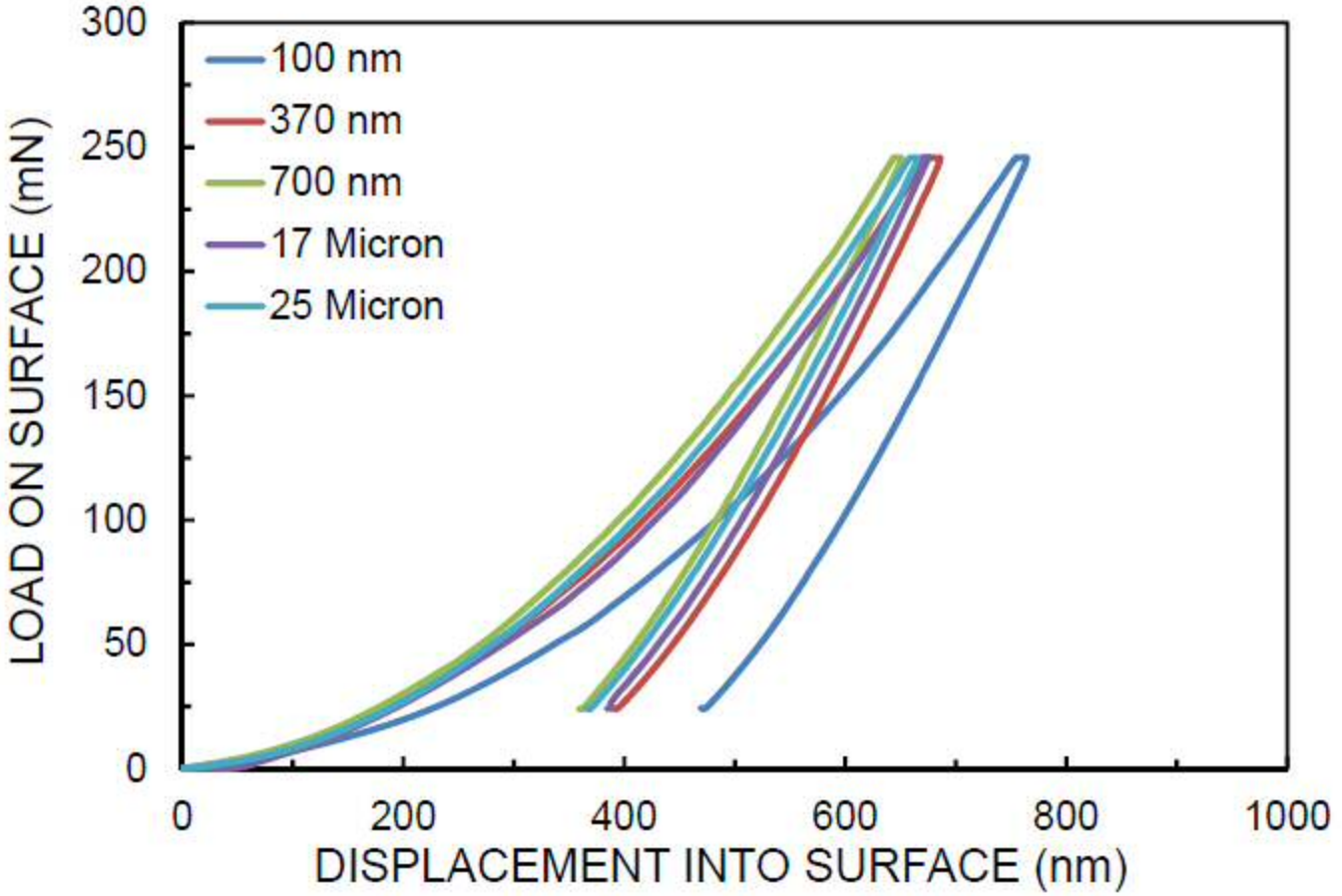
300
250
200
150
100
50
0
LOAD ON SURFACE (mN)
100 nm
370 nm
700 nm
17 Micron
25 Micron
0
200
400
600
800
1000
DISPLACEMENT INTO SURFACE (nm)

Fig. 2

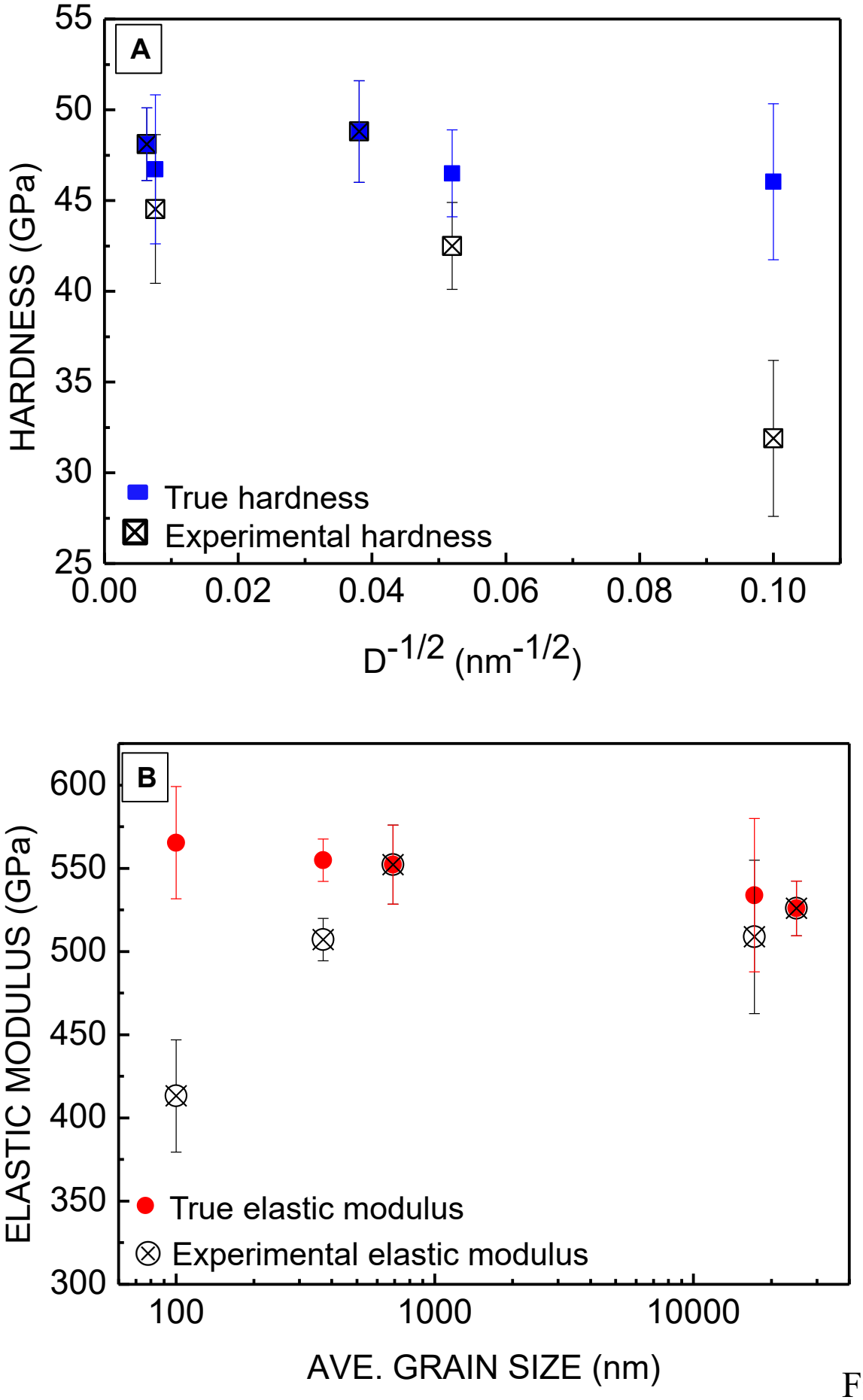
A
HARDNESS (GPa)
55
50
45
40
35
30
25
True hardness
Experimental hardness
0.00
0.02
0.04
0.06
0.08
0.10
D-1/2 (nm-1/2)
B
ELASTIC MODULUS (GPa)
600
550
500
450
400
350
300
True elastic modulus
Experimental elastic modulus
100
1000
10000
AVE. GRAIN SIZE (nm)

Fig. 3

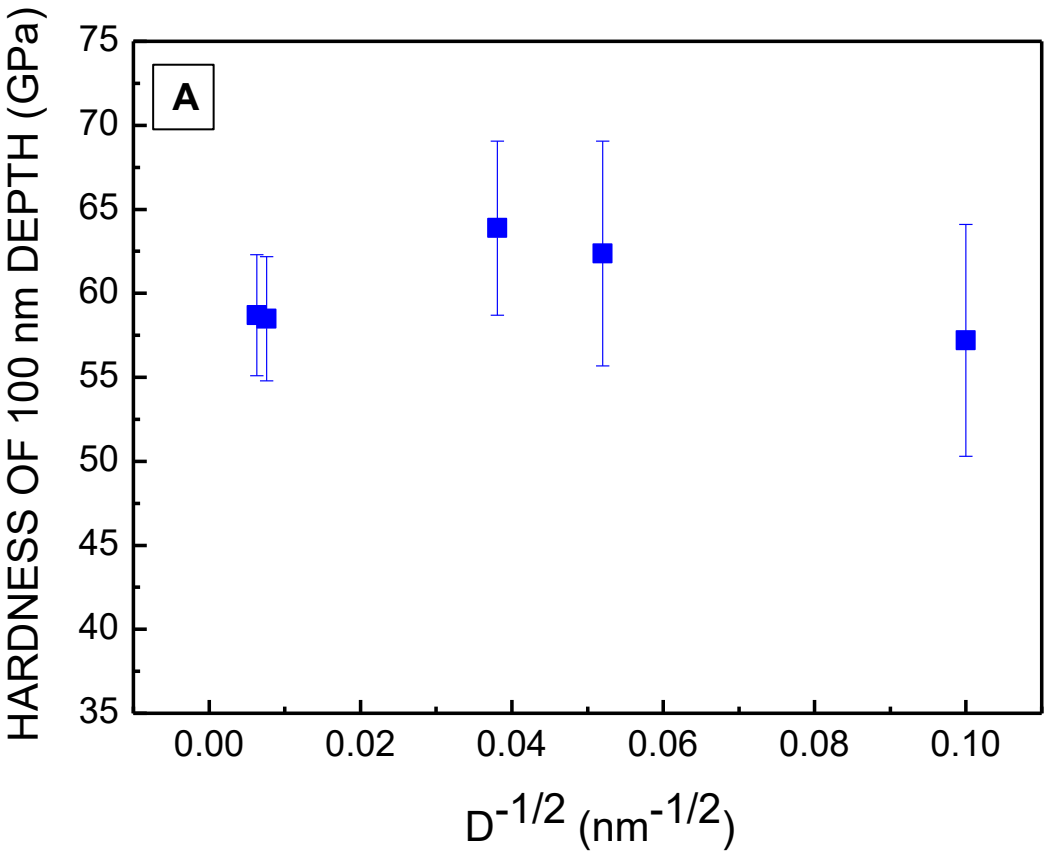
A
HARDNESS OF 100 nm DEPTH (GPa)
75
70
65
60
55
50
45
40
35
0.00
0.02
0.04
0.06
0.08
0.10
D-1/2 (nm-1/2)

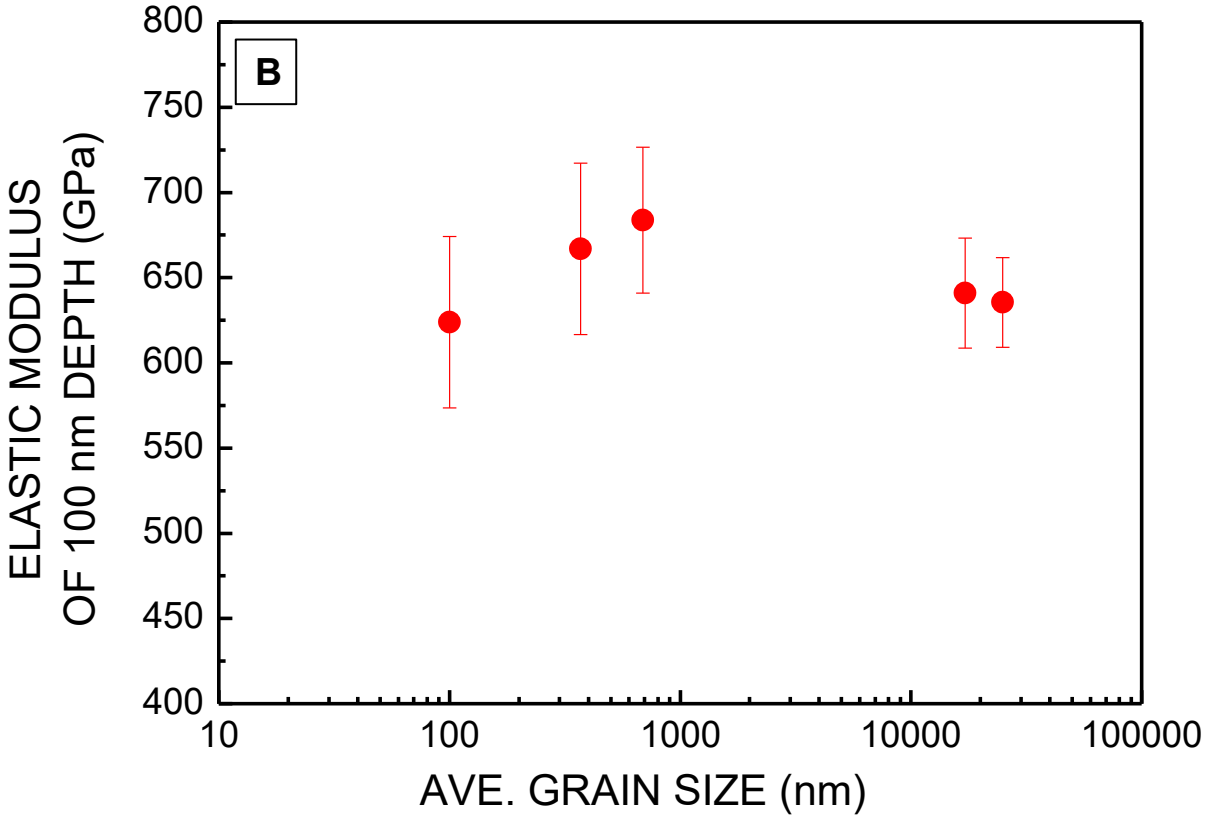
B
ELASTIC MODULUS
OF 100 nm DEPTH (GPa)
800
750
700
650
600
550
500
450
400
10
100
1000
10000
100000
AVE. GRAIN SIZE (nm)

Fig. 4

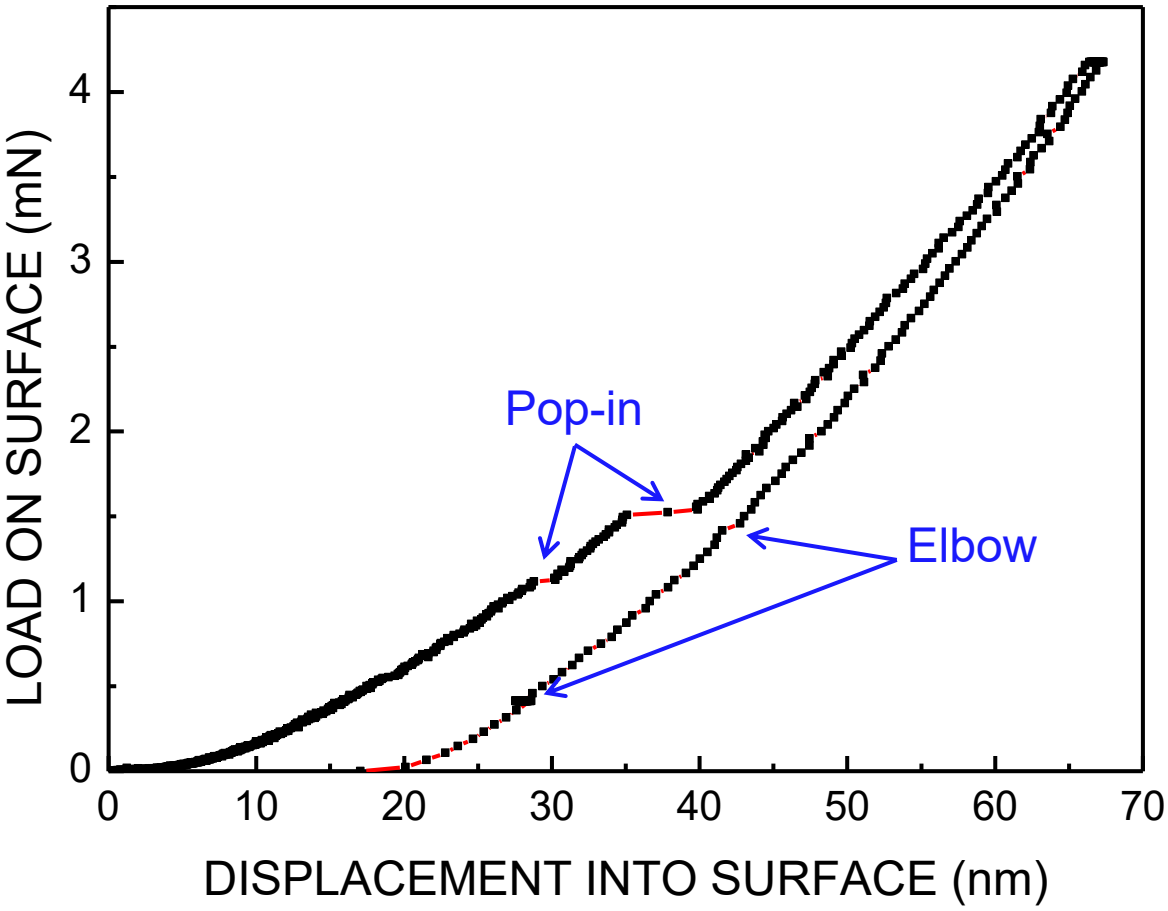
LOAD ON SURFACE (mN)
DISPLACEMENT INTO SURFACE (nm)
Pop-in
Elbow
0
1
2
3
4
0
10
20
30
40
50
60
70

Fig. 5

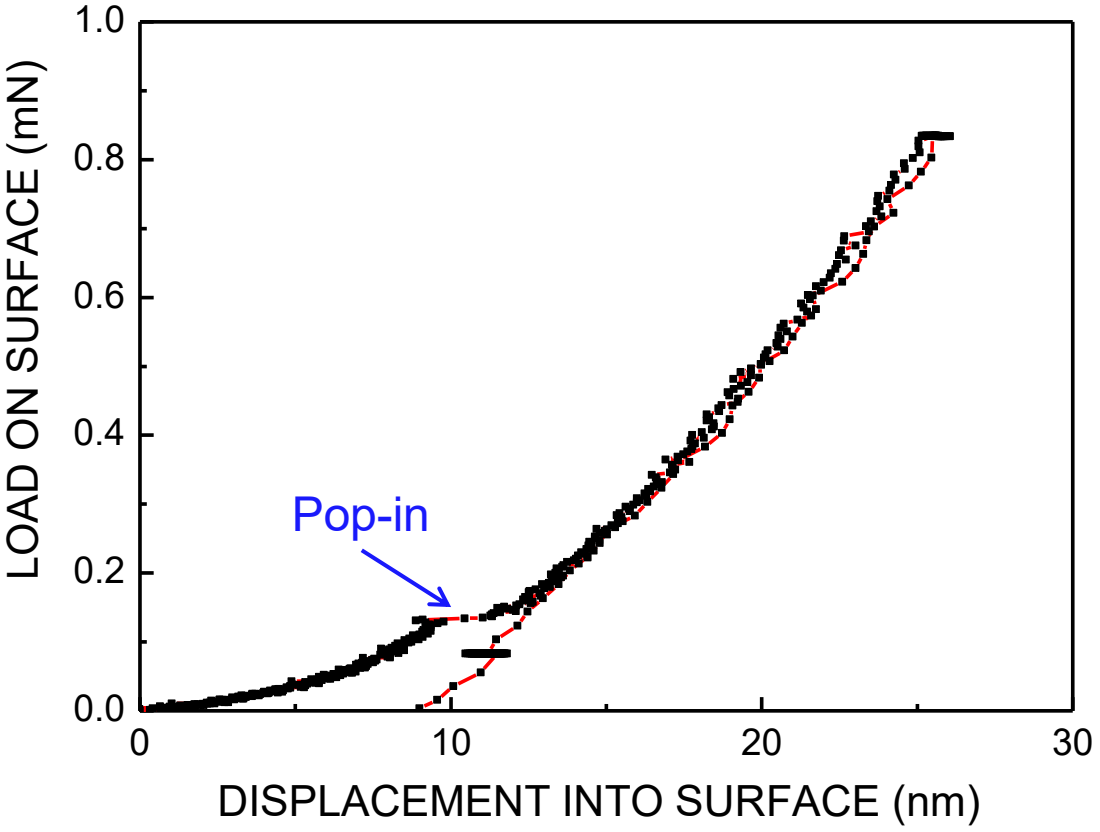
LOAD ON SURFACE (mN)
1.0
0.8
0.6
0.4
0.2
0.0
0
10
20
30
DISPLACEMENT INTO SURFACE (nm)
Pop-in

Fig. 6

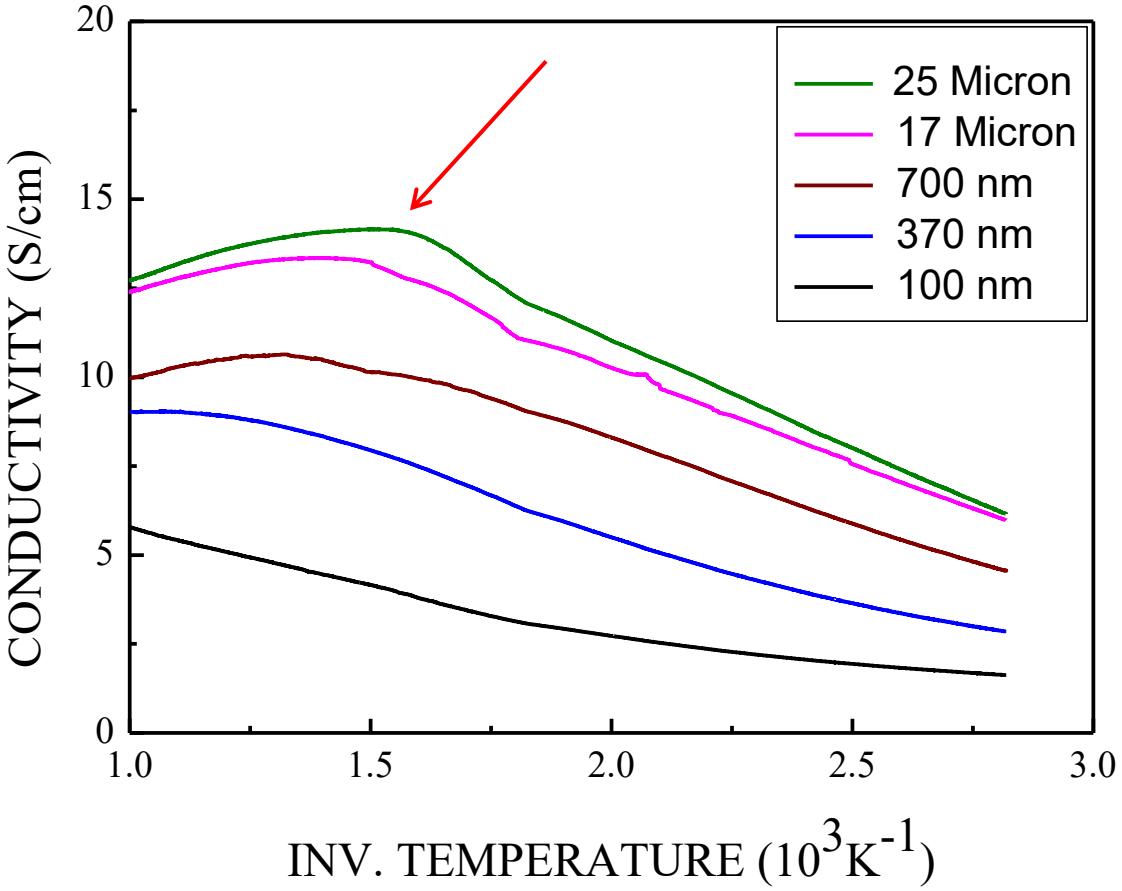
CONDUCTIVITY (S/cm)
INV. TEMPERATURE (10^3K^{-1})
25 Micron
17 Micron
700 nm
370 nm
100 nm
0
5
10
15
20
1.0
1.5
2.0
2.5
3.0

Fig. 7

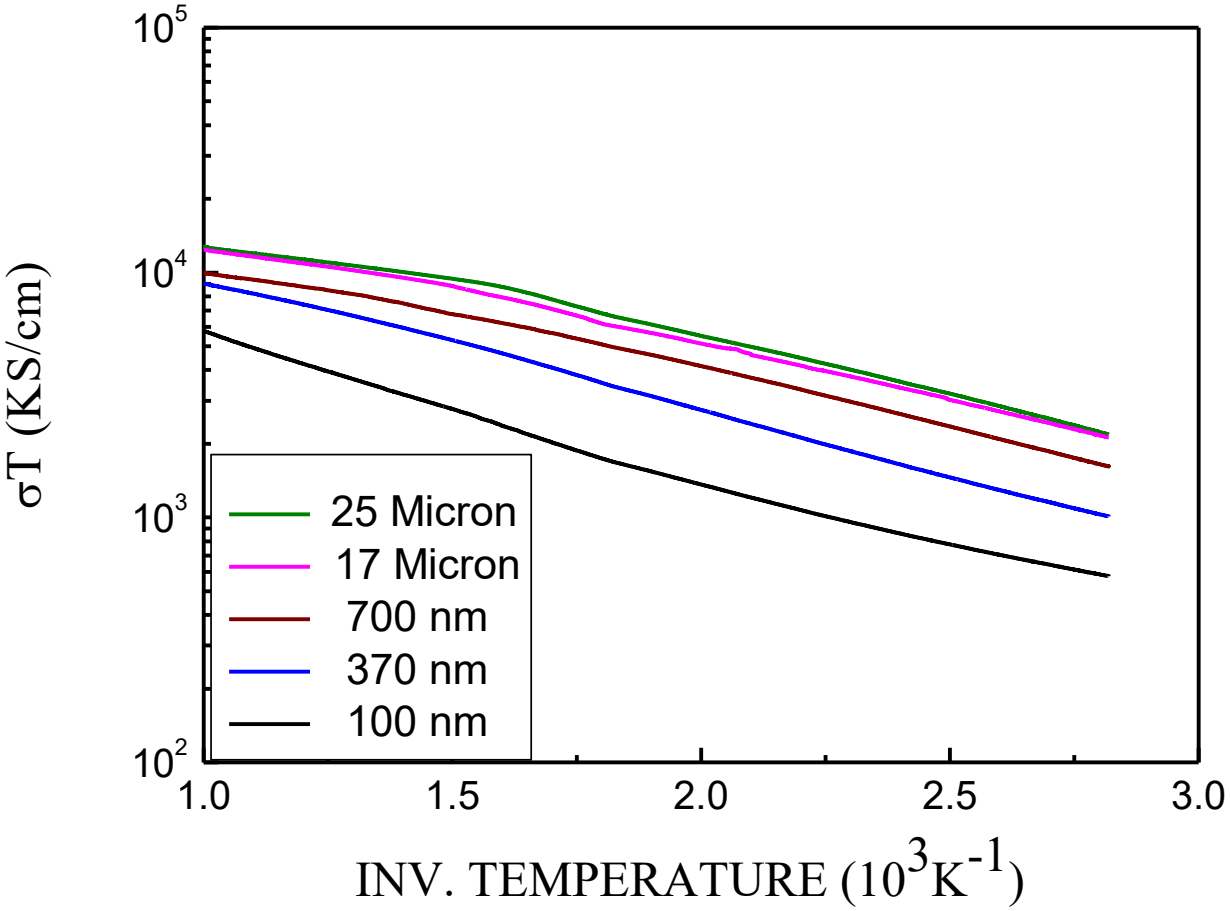
σT (KS/cm)
10^5
10^4
10^3
10^2
1.0
1.5
2.0
2.5
3.0
INV. TEMPERATURE (10^3K^-1)
25 Micron
17 Micron
700 nm
370 nm
100 nm

Fig. 8

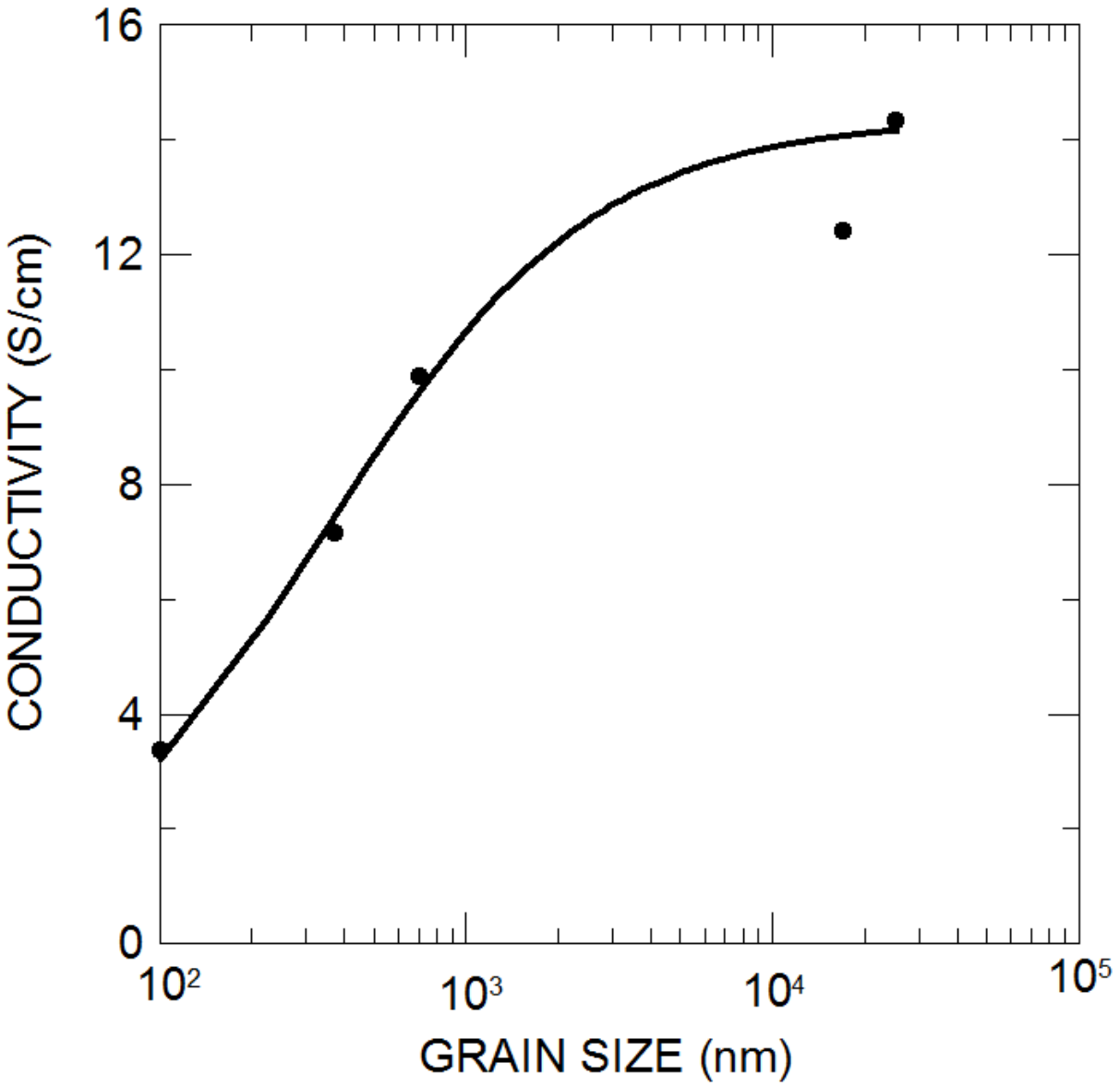

Fig. 9